American Mineralogist, Volume 73, pages 1255–1263, 1988

Stability of orthoenstatite at high temperature and low pressure

WILLIAM D. CARLSON
Department of Geological Sciences, University of Texas at Austin, Austin, Texas 78713, U.S.A.
J. STEVEN SWINNEA
Center for Materials Science and Engineering, University of Texas at Austin, Austin, Texas 78712, U.S.A.
DONALD E. MISER*
Department of Geological Sciences, University of Texas at Austin, Austin, Texas 78713, U.S.A.

ABSTRACT

Experimental evidence for the stability of synthetic Ca-bearing orthoenstatite near 1400 °C at atmospheric pressure in the system $Mg_2Si_2O_6$-$CaMgSi_2O_6$ is difficult to reconcile with other experimental results, given present thermodynamic models for pyroxenes on that join. The hypothesis that the phase stable under these conditions is not ordinary orthoenstatite, but is instead a structurally and mineralogically distinct phase, has been tested by optical, SEM, and TEM studies of crystals synthesized at 1370 °C and 1 atm, combined with a single-crystal X-ray structure refinement at 25 °C and with X-ray powder diffractometry at 25 °C and 1425–1440 °C. The results indicate that (1) the structure assumed by the quenched phase at room temperature is that of ordinary orthoenstatite and (2) the structure above 1400 °C is at least very similar to, and probably identical to, that of ordinary orthoenstatite and does not match the derivative structures seen at that temperature for analogous compositions of $Mg_2Si_2O_6$-$LiScSi_2O_6$ pyroxenes.

INTRODUCTION

The first reports of the appearance of an orthopyroxene-like Ca-bearing phase stable on the join $Mg_2Si_2O_6$-$CaMgSi_2O_6$ near 1400 °C at 1 bar (Schwab and Jablonski, 1973; Foster and Lin, 1975) were confirmed by the careful determination of its liquidus field in the system Mg_2SiO_4-$CaMgSi_2O_6$-SiO_2 by Longhi and Boudreau (1980). Although ensuing investigations have repeatedly reconfirmed the existence of this phase at low pressures and high temperatures (e.g., Jenner and Green, 1983; Biggar, 1985; Carlson, 1988), the identification of this material as orthoenstatite appears to contradict other experimental evidence and thermodynamic analysis. The principal difficulty lies in reconciling the breakdown near 1000 °C and 1 atm of orthoenstatite to protoenstatite + diopside, with the possible regeneration of orthoenstatite near 1400 °C and 1 atm by reaction of protoenstatite + pigeonite (Fig. 1). Schreinemakers' analysis of phase relations near the invariant point at which all four pyroxenes are stable (cf. Jenner and Green, 1983, p. 154; Biggar, 1985, p. 57–58; Carlson, 1985, p. 409–410; Carlson, 1988, Fig. 1) demonstrates that it is not possible for both of the above reactions to occur stably on the 1-atm isobar unless their reaction boundaries in P-T projection are strongly curved, which is unexpected for solid-solid reactions among these closely related pyroxene structures.

Jenner and Green (1983) attempted to resolve these contradictions by postulating 1-atm phase relations in which the assemblage protoenstatite + diopside was presumed to be nowhere stable; Biggar (1985) attempted the same by postulating 1-atm phase relations in which the assemblage orthoenstatite + diopside was presumed to be nowhere stable. Subsequently, however, experiments by Carlson (1985, 1986b, 1988) indicated that both assemblages are stable on the 1-atm isobar (Fig. 1). This result has forced a search for alternative explanations. The three most evident, considered in turn below, are (1) errors in the experimental determinations of phase equilibria; (2) thermochemical properties for low-Ca pyroxenes inconsistent with present thermodynamic models; and (3) the hypothesis that the phase stable near 1400 °C is a previously unrecognized pyroxene polymorph, structurally and mineralogically distinct from ordinary orthoenstatite. This article emphasizes data bearing upon the third of these possibilities. The designation "orthopyroxene" (Opx) is used here to refer to the phase stable near 1400 °C on the 1-atm isobar, whereas "orthoenstatite" (Oen) is reserved for reference to the familiar orthorhombic pyroxene, known to coexist with diopside at low temperatures on the 1-atm isobar and over large ranges of temperature at elevated pressures.

Phase equilibria

It is unlikely that the 1-atm phase equilibria are in serious error. Apparently conflicting evidence arises from three particular features of the phase-equilibrium exper-

* Present address: Departments of Geology and Chemistry, Arizona State University, Tempe, Arizona 85287, U.S.A.

0003–004X/88/1112–1255$02.00

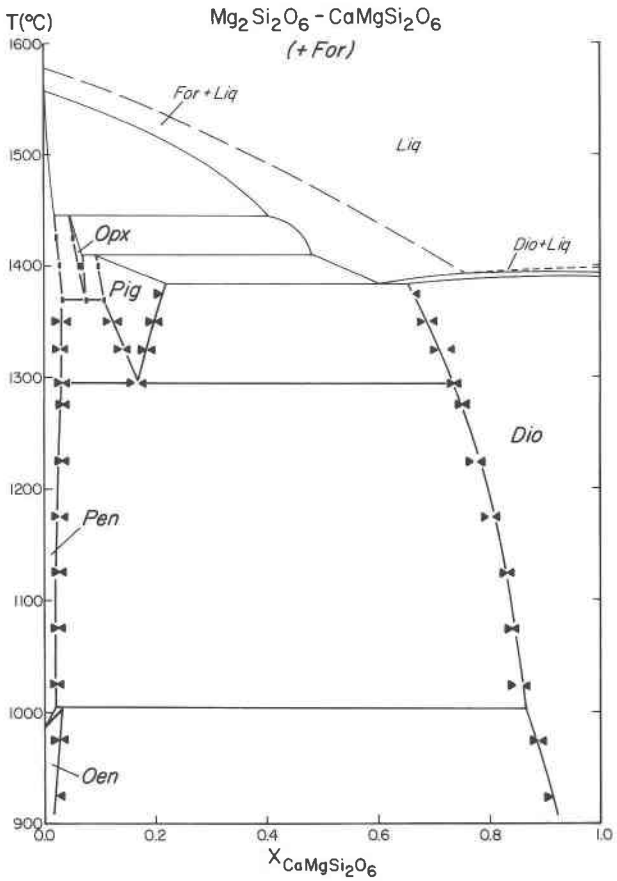

Fig. 1. Phase equilibria on the join $Mg_2Si_2O_6$-$CaMgSi_2O_6$ showing split stability field for phase(s) Oen and Opx. From Carlson (1988); supersolidus equilibria after Longhi and Boudreau (1980).

iments, but none is especially suspect. (1) The stable existence of Opx near 1400 °C seems incontrovertible, given the excellent agreement among several recent studies on the extent of stability of the phase (cf. Fig. 6 of Carlson, 1988). (2) Equilibrium at 1295 ± 10 °C among protoenstatite, pigeonite, and diopside is confirmed by the reversed experimental data of Carlson (1988), which correspond closely to synthesis data at higher temperatures from several sources (cf. Biggar, 1985). (3) Likewise, equilibrium at 1005 ± 10 °C among protoenstatite, orthoenstatite, and diopside is demonstrated by reversed experiments using a vanadate solvent (Carlson, 1985), which have been replicated, with identical results, using plumbate solvents (Carlson, 1988). These experiments corroborate the earlier synthesis results of Atlas (1952) and Boyd and Schairer (1964). Thus, although the rejection of any one of these three features would eliminate the apparent contradictions, all seem to be firmly based in experiment.

Thermodynamic analysis

It is possible that the thermodynamic properties of low-Ca pyroxenes in $Mg_2Si_2O_6$-$CaMgSi_2O_6$ are sufficiently unusual, and consequently poorly enough understood, to account for the split stability field for Oen shown in Figure 1. So far, however, no thermodynamic model for phase relations in this system has been able to reconcile that feature of the equilibria to the wealth of other experimental data in this system. The thermochemistry of pyroxenes in this system is extremely well constrained by reversed experimental data over the range 850–1600 °C and 1 atm–60 kbar and has been repeatedly modeled, with increasingly sophisticated thermodynamic formulations (e.g., Lindsley et al., 1981; Nickel and Brey, 1984; Carlson and Lindsley, 1988). Although the most recent of these models is capable of quantitatively reproducing all other features of the experimental phase equilibria, it does not generate an appropriate stability field at high temperature for Oen at 1-atm pressure. As detailed in Carlson and Lindsley (1988, p. 248) and as illustrated in Figure 2 by the location of the equilibrium "Oen = Pen + Pig," the assemblage protoenstatite + pigeonite is computed to be stable instead of orthoenstatite in the appropriate range of temperature and composition. There is no certainty that the thermodynamic formulation employed in these models is sufficiently complex to account for unusual thermodynamic properties of the low-Ca pyroxenes. Nevertheless, the fact remains that no modeling attempt so far has succeeded in accommodating the split stability field for Oen while simultaneously fitting the large amount of other data in this system.

Hypothesis of a distinct polymorph

The incompatibility between the experimental findings and present thermodynamic models focuses attention on a third possible explanation for the observations: perhaps the phase stable near 1400 °C is not ordinary orthoenstatite at all, but is instead a distinct entity. Such a hypothesis, if true, would reconcile the otherwise incompatible observations (cf. Carlson, 1985, p. 410–411). Although Longhi and Boudreau (1980) considered this possibility, they rejected it on the basis of the similarity of room-temperature X-ray powder-diffraction patterns of Oen and Opx.

The hypothesis is rendered somewhat more attractive, however, by the recognition of unusual derivative pyroxene structures in the analogous system $Mg_2Si_2O_6$-$LiScSi_2O_6$. At temperatures below about 1400 °C, the $Mg_2Si_2O_6$-$LiScSi_2O_6$ join comprises a sequence of phases isostructural with protoenstatite, orthoenstatite, pigeonite, and diopside (cf. Fig. 1 of Takéuchi et al., 1984), but with the structural variations extended over a wider range of compositions. Intriguingly, however, at temperatures near 1400 °C, a series of derivative structures appears for compositions near the magnesian end member (Takéuchi, 1978; Takéuchi et al., 1977, 1984). The derivative structures are characterized by planar slabs of material with *C*2/*c* clinopyroxene structure, varying with composition from 44.7 to 55.4 Å wide; these slabs are connected by narrow (~3-Å-wide) planar sheets of cross-linking octahedral sites (all vacant) and tetrahedra (30% vacant).

Successive slabs are reoriented relative to one another by glide operations. Variation in the width of the slabs allows these structures to maintain exact pyroxene stoichiometry over a range of compositions.

The resulting derivative structure has two features that would make it, or some closely related structure, appealing as an alternative for magnesian compositions in $Mg_2Si_2O_6$-$CaMgSi_2O_6$. First, the high vacancy content would account for the restriction of the derivative structure to high temperature and low pressure. Second, an ordinary clinopyroxene (CPX) structure can be transformed into the derivative structure "by a mechanism of cooperative atomic movements in the CPX structure which in effect leads to the polysynthetic twinning of the CPX structure" (Takéuchi, 1978, p. 176), in much the same way that protoenstatite can be transformed by minimal atomic repositioning into repetitively twinned clinoenstatite. This close relationship between alternative atomic positions might make the derivative structures (or, more likely, similar structures based on slabs of *Pbca* orthopyroxene) good candidates for either producing orthoenstatite-like X-ray patterns directly, or for inversion to orthoenstatite on cooling via an unquenchable phase transition.

Consequently, in order to test the hypothesis that the high-temperature Opx phase is distinct from Oen, and perhaps related to the derivative structures in $Mg_2Si_2O_6$-$LiScSi_2O_6$, we have attempted to characterize it by optical, X-ray, SEM, and TEM methods.

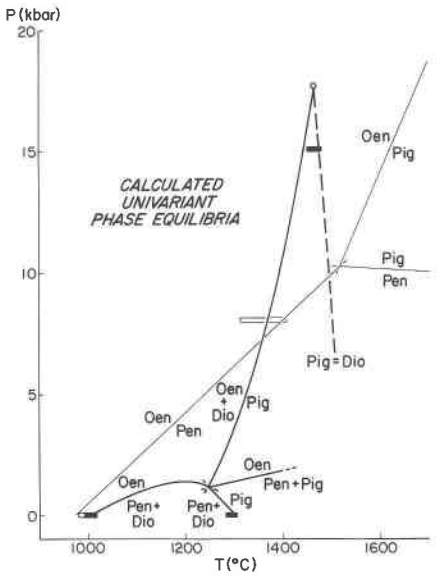

Fig. 2. *P-T* projections of calculated univariant reactions involving protoenstatite, orthoenstatite, pigeonite, and diopside (from Carlson and Lindsley, 1988), illustrating calculated stability of protoenstatite + pigeonite in place of orthoenstatite near 1400 °C and 1 bar. Bold lines depict ternary equilibria in CaO-MgO-SiO_2; lighter lines depict binary equilibria among the Ca-free end members. Equilibria are computed from a thermodynamic model constrained by experimental data indicated by rectangles and by additional data extending to 1600 °C and 60 kbar. Calculated supersolidus equilibria (metastable relative to silicate melts) at $T > \sim 1400$ °C and $P < \sim 5$ kbar are omitted.

Characterization of the high-temperature phase

Synthesis and chemical analysis

To synthesize crystals of sufficient size and suitable quality, the high-temperature solvent technique of Carlson (1986a) was employed. A sealed Pt capsule, containing equal weights of reactant glass and solvent with the compositions specified in Table 1, was maintained at 1370 ± 5 °C in a vertical quench furnace for 24 h and then dropped into water. A small chip of the charge was removed for analysis by electron microprobe, and the remainder was leached of quenched solvent-rich melt by immersion for 10–15 min in 4% HCl. Optical examination, X-ray powder diffraction, and microprobe analysis demonstrated that the crystalline run products consisted of 10 to 30-μm forsterite euhedra, 100 to 300-μm prisms of protoenstatite inverted to clinoenstatite (0.92 wt% CaO), 20 to 40-μm subhedral crystals of pigeonite (3.11 wt% CaO), and 50 to 300-μm euhedra of Opx. Both Opx and (to a lesser extent) protoenstatite commonly encompass tiny rounded inclusions of forsterite; other inclusions are rare.

Electron-microprobe analysis was performed by wavelength-dispersive techniques on a JEOL Superprobe 733, using an accelerating voltage of 15 kV, a sample current of 15 nA on brass, and counting intervals of 60 s on both peaks and backgrounds. Standards were NBS standard reference material #470 (glass K412) for Mg, Si, and Ca, and synthetic crystalline V_2O_5 for V; data reduction employed the empirical correction scheme of Albee and Ray (1970). The average of analyses at 25 randomly distributed points on seven grains of orthopyroxene in the run appears in the rightmost column of Table 1. That analysis is consistent with the range of compositions reported for this phase in other studies, as summarized in Biggar (1985).

Optical measurements

Crystals of Opx are distinguished from other phases in the run by their large size, gem clarity, and very pale blue color. It was therefore possible to extract crystals for optical, X-ray, SEM, and TEM analysis by hand-picking with forceps.

Fragments of crushed crystals display a distinct prismatic cleavage along two planes intersecting at an angle near 90°, but the best-developed crystal form is a pinacoid bisecting these cleavage planes; domal or sphenoidal terminations of the prisms are common. No twinning was observed, nor was there evidence of the fracturing along basal planes that is characteristic of inverted protoenstatite. Uncrushed grains tend to lie on the dominant pinacoid. These grains yield centered optic-normal figures of positive sign with γ oriented parallel to the trace of the approximately orthogonal cleavage planes. Crushed grain

Table 1. Compositions (wt%) of reactants and of Opx synthesized at 1370 °C and 1 atm

Oxide	Reactant glass	Solvent	Opx*
CaO	1.42	19.47	2.14
MgO	44.55	18.90	38.37
SiO_2	54.03	51.36	60.02
V_2O_5		10.27	0.10

* Average of 25 points over seven crystals.

mounts yielded several near-centered optic-axis figures, confirming the biaxial positive character of the phase and allowing estimation of the $2V$ as ~50°. These figures also display distinct optic-axis dispersion about the acute bisectrix of the sense $r > v$. The refractive indices α and γ were measured on uncrushed grains in immersion liquids using the dispersion-matching technique (Emmons and Gates, 1948). For wavelengths near Na_D, these indices are 1.654 and 1.661, respectively, with errors estimated at ±0.001; both indices show dispersion $n_F - n_C$ of approximately 0.017. The refractive index β was determined to be 1.658 ± 0.001 using immersion liquids and a crystal mounted on a spindle stage. These indices are in good agreement with determinations of birefringence calculated from measured thicknesses and retardations observed on oriented crystal fragments. All of the above optical properties are indistinguishable from those measured on Oen, the familiar orthoenstatite phase.

X-ray powder diffractometry at 25 °C

Four samples were examined by X-ray powder diffractometry at room temperature in this study; all were synthesized at atmospheric pressure and at temperatures from 1295 to 1370 °C in experiments similar to the synthesis run described above. These Opx compositions were chosen for analysis, despite the fact that they are probably metastable (cf. Carlson, 1988, p. 240), because they extend the range of measured CaO contents upward to nearly 3 wt%. All four samples produced diffraction patterns that could be satisfactorily indexed on the orthoenstatite structure. Unit-cell dimensions were refined from these powder patterns by a least-squares technique modified from that of Appleman and Evans (1973).

Cell dimensions from this study are compared in Figure 3 to data from several other sources. Formerly, only one measurement of cell parameters for the high-temperature Opx phase was available (filled diamonds). It falls well off the trend of the low-temperature Oen data (open squares and open triangles) and therefore was regarded as possible evidence for a distinct polymorph (cf. Fig. 3 of Carlson, 1985). The new determinations of cell parameters for Opx in this study (filled circles) fall closely on the trend of the Oen data and indicate that the data represented by the filled diamonds are discrepant. If the diamonds are disregarded, all data fall along a single trend, whether for crystals synthesized in the high-temperature Opx field (filled symbols) or for those synthesized under P-T conditions at which Oen is stable (open symbols).

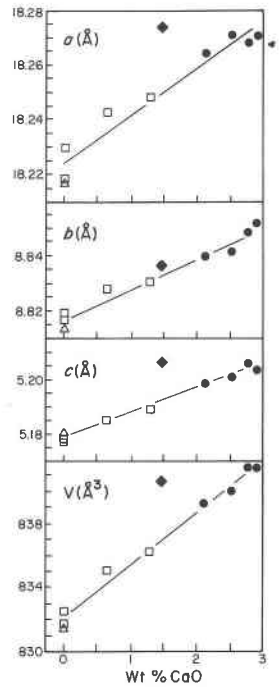

Fig. 3. Variations in unit-cell parameters at 25 °C with composition for Oen (shown by open symbols, synthesized at low temperatures and/or high pressures) and for Opx (shown by filled symbols, synthesized at high temperatures and 1-bar pressure). Shapes of symbols indicate sources of data: triangles from Hawthorne and Ito (1977); squares from Warner and Luth (1974); diamonds from Longhi and Boudreau (1980); and circles from this study.

Structure refinement at 25 °C on quenched crystal

To rule out the possibility that the quenched crystals possessed a derivative structure with differences from orthoenstatite too subtle to be revealed in powder-diffraction spectra, a single-crystal structure refinement at 25 °C was performed. The crystal selected for the refinement was gem-clear and subhedral, approximately 100 × 100 × 150 μm. Unfortunately, all of the large crystals contain inclusions of forsterite; the one chosen contained two rounded inclusions, each about 5 μm in diameter.

The crystal was mounted on a Syntex $P2_1$ automated diffractometer, and data were collected for $2\theta \leq 60°$, $0 \leq h \leq 25$, $0 \leq k \leq 12$, $-7 \leq l \leq 7$, using Mo$K\alpha$ radiation monochromatized with a graphite crystal, $\lambda = 0.71069$ Å. The diffractometer was operated in the ω-scan mode with scan rates varying from 4° to 8° min^{-1}. Four standard reflections (133, 352, $\bar{9}\bar{3}\bar{1}$, and $\bar{1}\bar{0}.\bar{3}\bar{1}$), collected after each 100 reflections, varied less than ±1% in intensity. Omega scans of several peaks were symmetric with peak widths at half-height of about 0.3°. A least-squares refinement of 30 reflections whose 2θ values were precisely determined in the range 25–30° yielded the lattice parameters $a = 18.280(2)$ Å, $b = 8.834(1)$ Å, $c = 5.197(1)$ Å. Measured intensities were transformed in the usual manner to structure amplitudes; no absorption correction was made. Es-

TABLE 2. Atomic positional and thermal parameters ($\times 10^4$) for 25 °C refinement

Site	x	y	z	U_{11}	U_{22}	U_{33}	U_{12}	U_{13}	U_{23}	U_{eq}
M1	3756(1)	6539(1)	8684(2)	68(4)	71(4)	64(4)	3(3)	−11(3)	2(3)	68(2)
M2*	3769(1)	4846(1)	3627(2)	93(5)	132(5)	74(5)	−21(3)	−19(3)	−17(3)	100(3)
SiA	2715(1)	3416(1)	495(1)	49(3)	53(3)	61(3)	−6(2)	5(2)	−4(2)	54(2)
SiB	4741(1)	3379(1)	7967(1)	52(3)	60(3)	59(3)	6(2)	2(2)	2(2)	57(2)
O1A	1834(1)	3399(2)	371(3)	49(7)	82(8)	62(8)	−1(6)	1(6)	−5(6)	64(5)
O2A	3107(1)	5019(2)	435(3)	85(8)	75(8)	73(8)	−16(6)	−10(6)	11(7)	78(5)
O3A	3027(1)	2249(2)	−1714(3)	75(8)	103(8)	89(8)	−5(7)	16(7)	−44(7)	89(5)
O1B	5627(1)	3403(2)	7981(3)	52(8)	89(8)	73(8)	−1(6)	−12(6)	1(6)	71(5)
O2B	4335(1)	4844(2)	6933(4)	103(9)	98(8)	99(8)	33(7)	15(7)	30(7)	100(5)
O3B	4478(1)	1986(2)	5988(3)	82(9)	114(8)	90(9)	−3(7)	−4(7)	−28(7)	95(5)

Note: The anisotropic thermal parameters in Å² are of the form $\exp[-2\pi^2(U_{11}a^{*2}h^2 + U_{22}b^{*2}k^2 + U_{33}c^{*2}l^2 + 2U_{12}a^*b^*hk + 2U_{13}a^*c^*hl + 2U_{23}b^*c^*kl)]$. $U_{eq} = \frac{1}{3}\Sigma_i U_{ii}$. Numbers in parentheses are estimated standard deviations.

* Refined M2 occupancy is 0.948 Mg and 0.052 Ca.

timated errors of the intensities were calculated from counting statistics. Equivalent reflections from the 2398 measured intensities were averaged to give 1223 unique reflections with $R_{int} = 0.0142$; of these, 1083 were considered observed on the basis that $F > 5\sigma_F$.

The structure was refined by full-matrix least-squares via SHELX-76 (Sheldrick, 1976). Initial atomic positions were taken from Hawthorne and Ito (1977). The 92 refined parameters included an overall scale factor, positional and anisotropic thermal parameters for all atoms, and the atomic fraction of Ca on the M2 site. Scattering factors were for neutral atoms corrected for the real and imaginary parts of dispersion (*International Tables for X-ray Crystallography,* 1974). For the observed reflections, the refinement converged to $R = 0.0303$ ($\omega R = 0.0319$), $S = 3.0$, $(\Delta/\sigma)_{max} = 0.005$, where $R \equiv (\Sigma|F_o - kF_c|)/\Sigma F_o$ and $\omega R \equiv (\Sigma\omega|F_o - kF_c|)/\Sigma\omega F_o$ with $\omega \equiv 5.6[\sigma^2(F) + 0.027F^2]^{-1}$. Using all reflections, the refinement converged to $R = 0.0355$ ($\omega R = 0.0340$). A final difference map gave random peaks $< |0.7$ e Å$^{-3}|$. The final positional and thermal parameters, which agree closely with those of Hawthorne and Ito (1977), are presented in Table 2. Table 3[1] contains a list of observed and calculated F as well as $\sigma(F_o)$. The refined occupancy of Ca in the M2 site is 5.2(7)%, in comparison with the average value of 7.7(1)% determined by the electron-microprobe analysis.

The quality of the fit leaves little doubt that the material recovered after quench is indeed ordinary orthoenstatite.

SEM and TEM observations

The data reported above leave open the possibility that a phase distinct from ordinary orthoenstatite exists at high temperature, but that it undergoes an unquenchable phase transition to Oen when cooled to room temperature. Scanning and transmission electron microscopic (SEM and TEM) observations bear on this possibility.

The SEM study was undertaken to confirm that the crystals' external morphology is orthorhombic. One unambiguous indication of inversion on quench from a different structure to orthoenstatite would be the preservation after quench of crystal morphology other than orthorhombic. However, the faces developed on all crystals that were examined in stereoscopic pairs of SEM photographs displayed orthorhombic symmetry.

The TEM study was undertaken principally to seek microstructural evidence of inversion through an unquenchable phase transition. Possible indications of such a transformation would include twinning and antiphase boundaries or other stacking faults. Most of the samples examined were prepared by crushing the pyroxenes (using the minimum force necessary to produce disaggregation) and dispersing the fragments onto holey C films. In order to evaluate the effects of deformation defects induced by sample preparation, two other techniques were also employed. Coarse crystals were embedded in epoxy and polished on a diamond lap to 30 μm thickness; these were then ion-thinned to obtain regions that were electron-transparent and to remove surface-related defects. Fine-grained crystals were likewise embedded in epoxy, but were ion-thinned without polishing to avert any deformation possibly arising from that procedure.

In TEM, the most common microstructure consists of numerous straight, fringed defects. These defects, which lie parallel to (100) as seen in Figure 4, generate pronounced streaking parallel to **a*** in electron-diffraction patterns. The defects are in contrast for most imaging conditions, but lose contrast for $\mathbf{g} = n \cdot 210$. Under these diffraction conditions, no residual strain contrast is observed; this indicates that the microstructure does not arise from nonstoichiometry. Although the defects resemble stacking faults, displacement vectors could not be determined from the available observations. The defects are most common at the edges of crushed grains (where they are associated with incipient parting and rotation), but many of the defects extend well into the interior of the crystals. Iijima and Buseck (1975), who examined similar defects in natural crystals, inferred that the high-density defects near the grain edges were induced by grinding during sample preparation, whereas defects ex-

[1] A copy of Table 3 may be ordered as Document AM-88-390 from the Business Office, Mineralogical Society of America, 1625 I Street, N.W., Suite 414, Washington, D.C. 20006, U.S.A.. Please remit $5.00 in advance for the microfiche.

Fig. 4. Typical straight defects parallel to (100) in synthetic Opx. Short dimension of image = 0.15 μm.

Fig. 5. Microstructure in synthetic Opx, consisting of irregular domains of opposite contrast (rarely observed). Two-beam dark-field image; short dimension = 30 μm; **g** = 832.

tending well into the grain were present prior to sample preparation. However, in all samples examined in this study, regardless of the method of preparation, defects occur both at grain edges and in grain interiors. Thus it appears that at least some of the defects are not artifacts of the preparation procedure.

Buseck and Iijima (1975) presented evidence that similar defects in natural Bamble bronzite are intergrowths of orthoenstatite and clinoenstatite induced by twinning during deformation by shear. In the synthetic samples, we observe many regions terminating entirely within the crystals that do not possess the 18-Å repeat distance characteristic of orthopyroxene. Only one lattice fringe is affected, consistent with the hypothesis that these regions are twin variants of orthopyroxene resulting in a clinoenstatite structure. It is possible that these regions originate from shearing during anisotropic contraction of the orthoenstatite on cooling. An alternative explanation, however, is that the thin lamellae represent growth defects on a growing (100) face. Optically visible striations on many of the crystals lend some support to the latter explanation. If such defects result from the normal growth of pyroxenes at elevated temperature, then the presence of these features, and of the parting that they induce, cannot alone be used as evidence for deformation. The measurement of clinoenstatite field widths, as suggested by Buseck and Iijima (1975), should be useful to distinguish between these two possibilities.

These defects, while numerous, occupy negligible volume and are spaced aperiodically. Consequently, they do not produce coherent scattering of X-rays and thus do not contribute, except as background, to the X-ray intensities measured in the refinement described previously. It is therefore not surprising to have obtained low values for R in the X-ray structure refinement, even though defects are almost certainly present in the material used in the single-crystal diffraction study.

In addition to the (100) defects, domains of opposite contrast separated by curvilinear boundaries were observed, as in the two-beam dark-field image (**g** = 832) shown in Figure 5. Irregular domain boundaries within a mineral of such striking anisotropy are characteristic of a texture induced on quench. Unfortunately, the features produce very weak contrast and were therefore only rarely observed. Their nature and origin are consequently poorly defined, and their presence, although perhaps suggestive of the development of antiphase domains, can-

not be regarded as compelling evidence for a phase inversion during quench.

X-ray powder diffractometry at 1425–1440 °C

X-ray powder diffractometry was used to examine directly the structure of the Opx phase at temperatures above 1400 °C. Spectra were obtained using Cu$K\alpha$ radiation over the range 10–70° 2θ, with powdered samples emplaced as an acetone slurry onto a Pt strip heater; the heater was equipped with a temperature controller calibrated against the melting points of NaCl, Ag, Au, and $CaMgSi_2O_6$. In addition to two Opx separates from the synthesis run described above, a specimen of natural bronzite from the Bamble, Norway, locality was also examined. After collecting an initial room-temperature spectrum, each sample was heated over an interval of about 1–2 min to 1440 °C, and a pattern obtained immediately; after approximately 1 h at this temperature, a second spectrum was collected at 1425 °C; after approximately 3 h at high temperature, a third pattern was run, again at 1440 °C. Each sample was then returned to room temperature and a final spectrum collected.

The high- and low-temperature spectra of the natural bronzite sample (which was immersed in an atmosphere of helium to prevent oxidation of Fe during the run) showed no marked differences, apart from the expected increase in cell parameters. Diffraction patterns of the synthetic material, however, showed distinct changes over time. The pattern run immediately after heating displayed broadened reflections of relatively low intensity. The two subsequent patterns, run after longer exposure to high temperature, both showed sharper and more intense reflections. These two spectra were nearly identical to each other, and although they closely resembled an orthoenstatite spectrum (as described in more detail below), both contained two diffraction maxima, of very low intensity, that are absent in the room-temperature spectra. The final room-temperature pattern matched the initial room-temperature spectrum very closely.

The high-temperature spectra strongly resemble the diffraction patterns of the natural orthoenstatite, suggesting that the structure of the phase at high temperature is closely related to that of Oen, if not identical to it. To attempt to determine whether the subtle differences that did appear are genuine indications of a difference in the high-temperature structure or are merely artifacts of the analysis, the powder pattern expected from end-member magnesian orthoenstatite at 1425 °C was calculated. The calculations were performed using the positional parameters of Hawthorne and Ito (1977), scattering factors for neutral atoms corrected for the real and imaginary parts of dispersion (*International Tables for X-ray Crystallography,* 1974), and cell parameters equal to those refined by a least-squares technique (after Appleman and Evans, 1973) from the observed 1425 °C powder pattern [in Å, $a = 18.567(4)$, $b = 8.954(2)$, $c = 5.341(6)$]. Table 4 compares the relative intensities of observed diffraction maxima with those calculated for the Oen structure at 1425 °C; except for 210, calculated maxima with $I/I_{100} < 1$ are omitted. The quantitative agreement is excellent, except for (a) excess intensity in the 210, 400, and 800 maxima, which is reasonably accounted for as the result of preferred orientation on cleavage and parting planes; (b) insufficient intensity (by a factor of three or greater) in the

Table 4. X-ray powder diffraction at 1425 °C

hkl	Obs 2θ	Calc 2θ	Obs I/I_{100}	Calc I/I_{100}
210	13.75	13.74	6	<1
400	19.15	19.12	6	1
020	19.85	19.85	5	12
211		21.60		2
	22.50		2	
121	26.45	26.42	8	23
411	27.35	27.33	10	13
420, 221	27.70	27.71	100	100
321	29.75	29.77	33	33
610	30.55	30.57	65	60
511	31.00	30.98	6	16
230	31.50	31.48	7	2
421	32.45	32.45	22	21
131, 202	34.90	34.89	75	78
521	35.65	35.67	7	25
302	36.70	36.63	3	5
331		37.45		4
800	38.90	38.82	28	2
711, 621	*	39.23	*	4
431	39.65	39.67	6	4
412	40.15	40.24	4	2
502	41.70	41.66	10	21
322	42.05	42.03	7	4
531	42.40	42.38	5	14
512, 721	43.00	42.98	5	13
811	43.75	43.77	4	3
141	44.15	44.13	3	7
440, 241	44.90	44.97	13	12
631	*	45.51	*	16
341	46.30	46.36	5	1
821	47.15	47.28	4	4
702		48.28		7
622		49.47		4
	49.85		6	
10.10	50.15	50.18	16	5
541		50.58		4
250	51.90	52.02	4	7
722, 831	52.75	52.80	7	9
812		53.31		7
142		53.65		1
242, 313	54.30	54.48	6	6
251		54.97		2
023, 123	55.50	55.64	3	22
902	56.30	56.36	3	6
931, 840	56.90	56.98	11	9
912	57.10	57.37	2	1
451	57.90	57.84	2	1
650, 12.00	59.50	59.74	5	10
922		60.35		2
133		60.79		19
10.31	61.20	61.33	10	18
642		61.83		1
060	62.15	62.21	3	7
352	64.45	64.44	2	7
11.02		65.38		9
11.31	65.90	65.95	9	16
11.12		66.33		4
723		66.65		2
043, 143		67.25		5
633		68.44		5
343		69.08		1

Note: Cu$K\alpha$ radiation; indexed on Oen structure.
* Interference from Pt sample holder.

121, 521, 023/123, and 133 maxima, for which no explanation is readily apparent; and (c) the expectable absence of several low-intensity reflections at high 2θ angles. A comparison between the observed diffraction pattern and a calculated powder pattern for the expanded derivative structure of Takéuchi et al. (1977) showed marked dissimilarities.

Under the hypothesis that the high-temperature structure is indeed that of ordinary orthoenstatite, only two features of the powder-diffraction data remain unexplained. (1) The initial degradation of the spectrum, and its subsequent improvement upon prolonged exposure to elevated temperature, may be the consequence of heating the crystal through a substantial range of temperature (1005–1370 °C) in which it is unstable, initially with respect to protoenstatite + diopside, and then with respect to protoenstatite + pigeonite. Although the heating was accomplished in only 1–2 min, incipient breakdown to the stable two-phase assemblages, followed by recovery of the pristine crystal structure, may have been responsible for the delay in establishing the stronger, sharper spectra. (2) Less easily explained is the appearance in all high-temperature patterns of two weak reflections that cannot be indexed on the Oen structure and that vanished after the sample was cooled to room temperature. It is likely that these reflections arose from small amounts of an additional phase produced during the diffraction experiment, but this cannot be confirmed. Calculated spectra of protoenstatite, clinoenstatite, and forsterite at 1425 °C indicate that it is unlikely that small amounts of one or more of these phases generate the two weak reflections. Although the origin of these two unindexed reflections remains uncertain, it seems unwise to seize upon them as the only indications of a possible structural variant at high temperature, especially in light of the otherwise excellent agreement expressed in Table 4.

Thermal expansion

If the high-temperature phase is indeed identical to Oen, then thermal-expansion coefficients calculated from the 25 °C and 1425 °C refinements of cell parameters should be consistent with those in the literature for other orthorhombic pyroxenes. The differences in cell parameters between 25 °C and 1425 °C generate mean linear coefficients of thermal expansion (in units of 10^{-5} per °C) of 1.12, 0.95, 1.98, and 4.14, for *a, b, c,* and volume, respectively. These values are similar in magnitude to those determined for orthoferrosilite (1.12, 1.09, 1.68, 3.93) by Sueno et al. (1976), for Ca-bearing ferrohypersthene (1.35, 1.45, 1.54, 4.38) by Smyth (1973), and for bronzite (1.64, 1.45, 1.68, 4.77) by Frisillo and Buljan (1972).

Conclusions

Although the evidence is not entirely unambiguous, this investigation strongly indicates that the orthopyroxene-like phase stable in $Mg_2Si_2O_6$-$CaMgSi_2O_6$ near 1400 °C at atmospheric pressure is identical to ordinary orthoenstatite. If it is not, it must possess a structure very similar to that of orthoenstatite and must invert to orthoenstatite on quench. Although it is conceivable that a derivative structure analogous to those in $Mg_2Si_2O_6$-$LiScSi_2O_6$ (perhaps with slabs of Oen in place of slabs of Cpx) might meet these criteria, such an explanation is probably unnecessary. A single-crystal X-ray structure refinement at ~1400 °C would, of course, still be valuable, as it should serve to remove any doubt about the identity of this phase.

An important implication of these findings is that, despite the progress made in our understanding of the thermochemistry of pyroxenes on the $Mg_2Si_2O_6$-$CaMgSi_2O_6$ join, still more accurate thermodynamic models for the low-Ca pyroxenes may be necessary to account for the complex phase relations seen at 1 atm. Further study of this problem should also include attempts to reliably determine phase equilibria in $Mg_2Si_2O_6$-$CaMgSi_2O_6$ at temperatures of 1000 to 1400 °C and pressures from 1 atm to 2 kbar. Such data might provide clues to the origin of the unusual thermodynamic behavior of low-Ca pyroxenes that now appears necessary to explain the phase equilibria at high temperatures and low pressures.

Acknowledgments

Support for this work was provided by NSF grants EAR-8603755 to W.D.C., and DMR-8520028 to H. Steinfink and J.S.S. of the Materials Science Laboratory. The Geology Foundation of the University of Texas at Austin helped to defray costs of publication. J. Longhi, D. H. Lindsley, and G. M. Biggar have contributed valuable discussions, correspondence, and criticism; T. L. Grove provided a helpful review. Both Biggar and Longhi graciously provided samples of their experimentally synthesized materials for analysis. Use of the high-temperature X-ray powder diffractometer was provided through the courtesy of the Corning Glass Works research facility in Corning, New York, and that work would not have been possible without the kindness and expertise of Bruce Aitken and John Geiger of Corning Glass Works, to whom we are especially grateful.

References Cited

Albee, A.L., and Ray, L. (1970) Correction factors for electron probe microanalysis of silicates, oxides, carbonates, phosphates, and sulfates. Analytical Chemistry, 42, 1408–1414.

Appleman, D.E., and Evans, H.T., Jr. (1973) Job 9214: Indexing and least squares refinement of powder diffraction data. U.S. National Technical Information Service, Document PB 216 188.

Atlas, L. (1952) The polymorphism of $MgSiO_3$ and solid-state equilibria in the system $MgSiO_3$-$CaMgSi_2O_6$. Journal of Geology, 60, 125–147.

Biggar, G.M. (1985) Calcium-poor pyroxenes: Phase relations in the system CaO-MgO-Al_2O_3-SiO_2. Mineralogical Magazine, 49, 49–58.

Boyd, F.R., and Schairer, J.F. (1964) The system $MgSiO_3$-$CaMgSi_2O_6$. Journal of Petrology, 5, 275–309.

Buseck, P.R., and Iijima, S. (1975) High resolution electron microscopy of enstatite. II: Geological application. American Mineralogist, 60, 771–784.

Carlson, W.D. (1985) Evidence against the stability of orthoenstatite above ~1005 °C at atmospheric pressure in CaO-MgO-SiO_2. Geophysical Research Letters, 12, 409–411.

——— (1986a) Vanadium pentoxide as a high-temperature solvent for phase equilibrium studies in CaO-MgO-Al_2O_3-SiO_2. Contributions to Mineralogy and Petrology, 92, 89–92.

——— (1986b) Reversed pyroxene phase equilibria in CaO-MgO-SiO_2 at one atmosphere pressure. Contributions to Mineralogy and Petrology, 92, 218–224.

——— (1988) Subsolidus phase equilibria on the forsterite-saturated join $Mg_2Si_2O_6$-$CaMgSi_2O_6$ at atmospheric pressure. American Mineralogist, 73, 232–241.

Carlson, W.D., and Lindsley, D.H. (1988) Thermochemistry of pyroxenes on the join $Mg_2Si_2O_6$-$CaMgSi_2O_6$. American Mineralogist, 73, 242–252.

Emmons, R.C., and Gates, R.M. (1948) The use of Becke line colors in refractive index determination. American Mineralogist, 33, 612–618.

Foster, W.R., and Lin, H.C. (1975) New data on the forsterite-diopside-silica system. EOS, 56,470.

Frisillo, A.L., and Buljan, S.T. (1972) Linear thermal expansion coefficients of orthopyroxene to 1000 °C. Journal of Geophysical Research, 77, 7115–7117.

Hawthorne, F.C., and Ito, J. (1977) Synthesis and crystal-structure refinement of transition-metal orthopyroxenes. I: Orthoenstatite and (Mg,Mn,Co) orthopyroxene. Canadian Mineralogist, 15, 321–338.

Iijima, S., and Buseck, P.R. (1975) High resolution electron microscopy of enstatite. I: Twinning, polymorphism, and polytypism. American Mineralogist, 60, 758–770.

International Tables for X-ray Crystallography. (1974) Volume IV. Kynoch Press, Birmingham, England.

Jenner, G.A., and Green, D.H. (1983) Equilibria in the Mg-rich part of the pyroxene quadrilateral. Mineralogical Magazine, 47, 153–160.

Lindsley, D.H., Grover, J.E., and Davidson, P.M. (1981) The thermodynamics of the $Mg_2Si_2O_6$-$CaMgSi_2O_6$ join: A review and an improved model. In R.C. Newton, A. Navrotsky, and B.J. Wood, Eds., Thermodynamics of minerals and melts, p. 149–175. Springer-Verlag, New York.

Longhi, J., and Boudreau, A.E. (1980) The orthoenstatite liquidus field in the system forsterite-diopside-silica at one atmosphere. American Mineralogist, 65, 563–573.

Nickel, K.G., and Brey, G. (1984) Subsolidus orthopyroxene-clinopyroxene systematics in the system CaO-MgO-SiO_2 to 60 kbar: A re-evaluation of the regular solution model. Contributions to Mineralogy and Petrology, 87, 35–42.

Schwab, R.G., and Jablonski, K.H. (1973) Der Polymorphismus der Pigeonite. Fortschritte der Mineralogie, 50, 223–263.

Sheldrick, G.M. (1976) SHELX-76: A program for crystal structure determination. University Chemical Laboratory, Cambridge, England.

Smyth, J.R. (1973) An orthopyroxene structure up to 850 °C. American Mineralogist, 58, 636–648.

Sueno, S., Cameron, M., and Prewitt, C.T. (1976) Orthoferrosilite: High-temperature crystal chemistry. American Mineralogist, 61, 38–53.

Takéuchi, Y. (1978) 'Tropochemical twinning': A mechanism of building complex structures. Recent Progress of Natural Sciences in Japan, 3, 153–181.

Takéuchi, Y., Kudoh, Y., and Ito, J. (1977) High-temperature derivative structure of pyroxene. Proceedings of the Japan Academy, Series B, 53, 60–63.

——— (1984) New series of superstructures based on a clinopyroxene. I. The structure of the 'enstatite-IV' series, $[Mg_{(x-12)/3}Sc_4][Li_{4/3}Si_{(x-4)/3}]O_x$, with $x = 100$, 112 or 124. Acta Crystallographica, B40, 115–125.

Warner, R.D., and Luth, W.L. (1974) The diopside-orthoenstatite two-phase region in the system $CaMgSi_2O_6$-$Mg_2Si_2O_6$. American Mineralogist, 59, 98–109.

Manuscript received February 1, 1988
Manuscript accepted July 27, 1988